ADVANCED MATERIALS INTERFACES
Open Access
www.advmatinterfaces.de

Unlocking the Potential of Sub-Nanometer Pd Catalysts for Electrochemical Hydrogen Peroxide Production

Ji Sik Choi, Suhwan Yoo, Ezra S. Koh, Raquel Aymerich-Armengol, Christina Scheu, Guilherme V. Fortunato, Marcos R. V. Lanza, Yun Jeong Hwang,* and Marc Ledendecker**

The utilization of nanoscale catalysts represents a valuable and promising strategy for augmenting catalytic performance while mitigating the reliance on expensive noble metals. Nevertheless, a significant knowledge gap persists regarding the intricate interplay between catalyst size, physical properties, and catalytic behavior in the context of the oxygen reduction reaction. In this study, the synthesis of precisely controlled palladium catalysts is presented, spanning a wide range from individual atoms to metal clusters and nanoparticles, followed by a comprehensive evaluation of their performance in acidic conditions. The results show a significant increase in H_2O_2 selectivity of up to 96% with decreasing catalyst size and strategic approaches are identified to eliminate unselective sites, facilitating the attainment of active and selective catalysts. The enhanced selectivity of the catalysts highlights the potential of single atom catalytic sites and can be adapted to improve the performance of various catalytic processes.

1. Introduction

The development of catalysts with well-defined sizes, surface facets, and ligand environments has gained significant attention in catalysis in recent years.[1–5] The catalytic and physical properties are fundamentally altered as the size of the metal cluster is reduced further to a sub-nanometer scale and ultimately to an atomic level.[6] As a result, metal clusters and single atom materials have received much attention in recent years as they allow for precise control of the number and quality of active sites leading to potentially higher catalytic activity and selectivity compared to their bulk counterparts, resulting in improved efficiency and cost-effectiveness in the production process. Especially, competitive catalytic reactions can be selectively tuned depending on the nature of the atomic level active sites. Researchers have synthesized various nanoparticles, clusters, and single atom catalysts using metals such as Pt, Pd, and Au, with many studies focusing on the optimization of their metal loading, size, shape, and surface properties to improve catalytic performance.[7–12]

The catalytic understanding and differentiation between single atoms, clusters, and nanoparticles is laborious and poses challenges for their widespread use in a variety of applications.[13,14] This is especially true for the production of hydrogen peroxide where extended surfaces lead to the decomposition of H_2O_2 to H_2O.[15–17] Size effects in fuel cell research have received extensive attention in the last decades focusing on the 4-electron pathway toward water.[1,2,7,18–21] While metal clusters and single atom catalysts essentially eliminate the presence of metallic sites that are typically present in bulk catalysts, their selectivity and activity toward hydrogen peroxide only received minor attention so far.[3,22–24]

J. S. Choi, G. V. Fortunato, M. Ledendecker
Department of Chemistry
Technical University of Darmstadt
64287 Darmstadt, Germany
E-mail: jisik.choi@tu-darmstadt.de; marc.ledendecker@tum.de

J. S. Choi, E. S. Koh, G. V. Fortunato, M. Ledendecker
TUM Campus Straubing for Biotechnology and Sustainability
Technical University of Munich
94315 Straubing, Germany

S. Yoo, Y. J. Hwang
Department of Chemistry
Seoul National University (SNU)
Seoul 08826, Republic of Korea
E-mail: yjhwang1@snu.ac.kr

R. Aymerich-Armengol, C. Scheu
Nanoanalytics and Interfaces
Max-Planck-Institut für Eisenforschung GmbH
40237 Düsseldorf, Germany

G. V. Fortunato, M. R. V. Lanza
Institute of Chemistry of São Carlos
University of São Paulo
São Carlos, SP 13566–590, Brazil

Y. J. Hwang
Center for Nanoparticle Research
Institute for Basic Science (IBS)
Seoul 08826, Republic of Korea

The ORCID identification number(s) for the author(s) of this article can be found under https://doi.org/10.1002/admi.202300647

DOI: 10.1002/admi.202300647

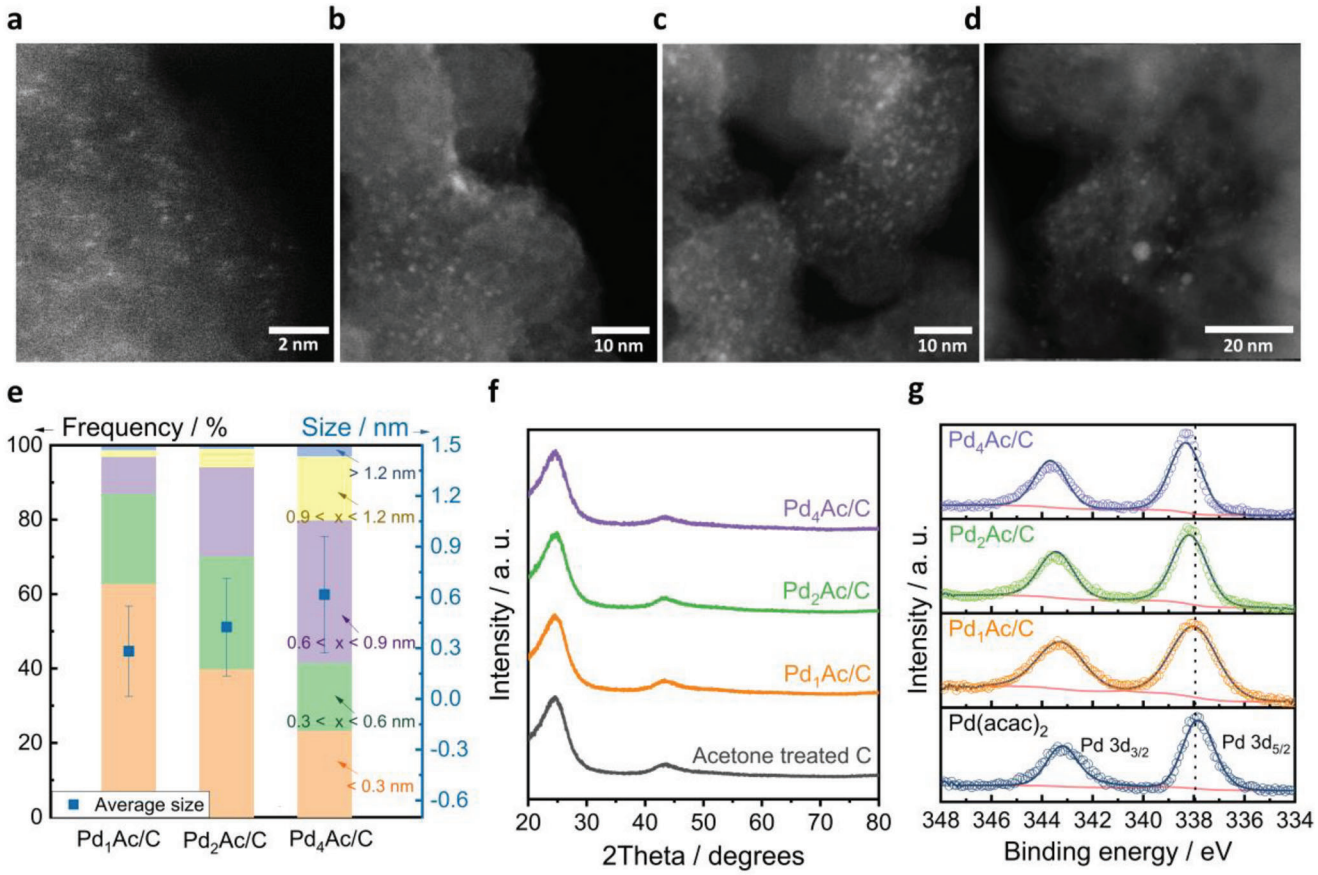

Figure 1. Characterizations of Pd_xAc/C catalysts. HAADF-/STEM images of a) Pd_1Ac/C, b) Pd_2Ac/C, c) Pd_4Ac/C, and d) Pd_{NPs}/C. The scale bars for (a–d) are 2 nm, 10 nm, 10 nm, and 20 nm, respectively. e) Stacked histogram of the frequency particle size distributions and average cluster diameters. f) XRD patterns. g) Core level XPS spectra corresponding to the Pd 3d core level of Pd clusters.

Our study aims to elucidate the electrochemical performance of metal nanoparticles, metal clusters, and single atoms, with the objective of unraveling the underlying mechanisms that contribute to achieving high selectivities in the hydrogen peroxide production. Specifically, a diverse array of catalysts was synthesized utilizing an organic metal precursor impregnation method. These catalysts were tailored to exhibit a range of sizes, enabling us to systematically investigate the influence of size distribution on catalytic performance. To correlate the underlying mechanisms governing the observed performance variations with the structural characteristics of the catalysts, we employed high angle annular dark field high-resolution scanning transmission electron microscopy (HAADF-STEM). To further enhance our understanding, we utilized in situ/operando electrochemical attenuated total reflection-surface enhanced infrared reflection absorption spectroscopy (ATR-SEIRAS) in order to explore the active and selective sites present within the catalysts. To accomplish this, we introduced carbon monoxide (CO) as a probe molecule, strategically designed to mask any unselective catalytic sites. By modifying the direct environment at the metal/electrolyte interface, we established a correlation between the vibrational signatures of CO and the specific behavior of the oxygen reduction reaction (ORR).

2. Results and Discussion

In order to correlate the ORR activity and selectivity in relation to atomic cluster size, a series of palladium catalysts supported on carbon (designated as Pd_xAc/C, with x representing the Pd loading in wt.%) were prepared. The catalysts were prepared through a wet impregnation method, utilizing palladium acetylacetonate impregnated onto Vulcan XC72R carbon support.

To ascertain the particle size distribution of the prepared catalysts, an in-depth characterization was performed employing HAADF. **Figure 1**a–c and Figure 1e show the HAADF-STEM images, accompanied by stacked histograms illustrating the frequency size distribution and average cluster diameters. For Pd_1Ac/C, the Pd speciation revealed predominantly atomically dispersed metal sites accompanied by a smaller fraction of di/trimeric Pd species. Negligible amounts of nanoparticles with diameters smaller than 1.2 nm were detected. The average cluster diameters for Pd_1Ac/C, Pd_2Ac/C, Pd_4Ac/C, and Pd_{NPs}/C were 0.28 ± 0.26 nm, 0.43 ± 0.29 nm, 0.62 ± 0.34 nm and 2.46 ± 2.27 nm, respectively (Figure S1, Supporting Information). In addition to Pd clusters, Pd single atoms were observed in all samples (Figure S2, Supporting Information). These findings

highlight the controlled synthesis of catalysts with distinct atomic cluster sizes, allowing for a systematic investigation of their impact on catalytic performance. In addition to size distribution, the Pd content in the synthesized catalysts was quantified using X-ray fluorescence (XRF) analysis, yielding measured values of 0.89% for Pd_1Ac/C, 1.53% for Pd_2Ac/C, and 3.03% for Pd_4Ac/C (Table S1, Supporting Information).

After confirming the successful manipulation of average Pd cluster size, XRD and XPS were applied to gain a comprehensive understanding of the physical and chemical properties of the deposited Pd catalysts and their surface speciation after synthesis. The XRD spectra for various as-prepared Pd atomic cluster catalysts and acetone treated carbon are shown in Figure 1f. Notably, for both single atom and cluster catalysts, no discernible diffractions corresponding to metallic Pd (JCPDS no. 46–1043) or PdO (JCPDS no. 41–1107) were detected. The broad and weak diffractions at ≈25° and 43° 2Theta correspond to amorphous carbon.[25] High-resolution XPS was used to study the oxidation state of Pd. Figure 1g showcases the Pd 3d core-level spectra for Pd_xAc/C ($x = 1$, 2, and 4) after peak deconvolution. The XPS spectra of the Pd 3d level are characterized by the spin-orbit split components corresponding to the Pd $3d_{3/2}$ and Pd $3d_{5/2}$ doublets. Analysis of the Pd $3d_{5/2}$ peaks revealed peak positions at 338.0, 338.2, and 338.3 eV for Pd_1Ac/C, Pd_2Ac/C, and Pd_4Ac/C, respectively, indicative of oxidized Pd species, $Pd^{\delta+}$ with $2 \leq \delta \leq 4$.[26] Consistent with the XRD analysis, no secondary metallic Pd speciation at 335.3 eV was detected.[27] To gain insights into the embedding coordination environment of the Pd catalysts, we included bare $Pd(acac)_2$ as a reference in our analysis. The obtained signals at 338.0 eV are in agreement with literature ranging between 337.9 and 338.3 eV[27,28] validating the retention of Pd^{2+} and supporting the intact deposition of the acetylacetonate complex.[26]

To ensure the stability of the prepared catalysts during the electrochemical study, we compared the initial cyclic voltammograms of Pd_1Ac/C and Pd_4Ac/C in the potential range of 0.1 and 0.9 V_{RHE}. Additionally, XPS before and after the ORR were recorded. In Figure S3 (Supporting Information), we observed no characteristic oxidation peak associated with the decomposition of $Pd(acac)_2$ or any other indications of Pd_1Ac/C electrochemical reduction/oxidation, whereas Pd_4Ac/C showed a minor reduction peak, attributed to the small share of nanoparticles where surface oxidation and reduction occurs. This is in line with the particle size distribution shown in Figure 1e. Furthermore, in Figure S4 (Supporting Information), XPS spectra obtained after the ORR provide additional support for the stability of the catalysts during the electrochemical study. Specifically, Pd_1Ac/C showed no significant phase changes, with only a slight downshift of 0.08 eV in the Pd $3d_{5/2}$ binding energy compared to the initial state. In contrast, Pd_4Ac/C displayed partial reduction to metallic Pd (Pd^0) with a binding energy of 335.7 eV, consistent with the cyclic voltammograms shown in Figure S3 (Supporting Information). The proportion of metallic Pd following reduction, as determined by XPS analysis, aligns with the fraction of particles larger than 1 nm as indicated by the acquired particle size distribution. These observations suggest that smaller-sized Pd particles below 1 nm in the Pd_xAc/C, which strongly interact with the acetylacetonate ligand, exhibit hindered reduction, while larger-sized Pd particles, over 1 nm, are more prone to reduction. Considering the combined results of the XPS analysis after the ORR and the absence of Pd oxidation peaks in the initial current-potential curves, we can conclude that the electrochemical reduction of $Pd(acac)_2$ did not occur.

In order to correlate the influence of the cluster size with its electrocatalytic performance, ORR polarization curves were recorded in an O_2-saturated 0.1 M $HClO_4$ electrolyte between 0.1 and 0.9 V_{RHE} at forced convection of 1600 rpm. To ensure consistency in the electrocatalysis experiments, a constant Pd loading of 10 μg cm^{-2} was employed on the working electrode. The acetone-treated carbon as a reference showed nearly no activity within the applied potential range of 0.1–0.6 V_{RHE} as shown in **Figure 2**a. For Pd_{NPs}/C, the ORR polarization curves align with previous reports on palladium nanoparticles with low selectivity of 7.7% toward H_2O_2 over the whole potential range. The polarization curves demonstrate a well-established diffusion limiting regime below 0.6 V_{RHE}, indicating a 4-electron process.[29] The ORR onset potential, as depicted in Figure 2a, is shifted from 0.89 V_{RHE} for Pd_4Ac/C to 0.86 V_{RHE} for Pd_2Ac/C and 0.71 V_{RHE} for Pd_1Ac/C, close to the thermodynamically expected potential of H_2O_2 production ($E^0_{O_2/H_2O_2} = 0.69$ V_{SHE}).

The corresponding H_2O_2 selectivity as determined by Equation S1 (Supporting Information), and electron transfer numbers (denoted as n and calculated using Equation S2 (Supporting Information), averaged between 0.1 and 0.5 V_{RHE}, were plotted as a function of the cluster size in Figure 2b. Pd_1Ac/C exhibited H_2O_2 selectivities of 86%, while Pd_2Ac/C and Pd_4Ac/C produce H_2O_2 with 43% and 21% selectivity, respectively. The number of transferred electrons n for Pd_1Ac/C was calculated to be ≈2.3 averaged between 0.1 and 0.5 V_{RHE}, indicating a dominant 2-electron pathway. In contrast, Pd_2Ac/C and Pd_4Ac/C had n values of 3.1 and 3.6, suggesting an increased contribution from a 4-electron pathway.

The ORR selectivity to H_2O_2 increases proportionally with a decrease in particle/cluster size, which is closely linked to the oxidation state and size of Pd. The presence of acetylacetonate ligands might introduce geometric modifications to the metal, which, in turn, influence the oxygen adsorption behavior on the catalyst surface. From literature, the ligands predominantly facilitate end-on O_2 adsorption on Pd.[30–32] Once O_2 adsorbs in an end-on configuration, only one reaction intermediate, OOH*, is involved, and as a result, both catalytic activity and selectivity are mostly determined by the binding free energy of the OOH* intermediate.[10,33] High-resolution XPS analysis of the Pd 3d spectrum revealed that the binding energy of Pd $3d_{5/2}$ in Pd_1Ac/C measured at 338.0 eV is higher compared to metallic Pd situated at 335.3 eV, strongly indicating an electron transfer from Pd to acetylacetonate. This leads to modifications in the electronic structure of Pd, which could result in a downshift of the metals d-band center. As a consequence, the lowered d-band center influences the binding energy and impacts the adsorption/desorption behavior of the reaction intermediate on Pd sites, potentially weakening the binding energy of the reaction intermediate.[34–36] As a result, the reaction primarily proceeds through the dominant 2-electron pathway. While the binding energy of Pd $3d_{5/2}$ in Pd_4Ac/C experienced a significant upward shift compared to Pd_1Ac/C, the catalytic behavior showed an opposite trend due to the extended Pd surface resulting from an increase in cluster size.

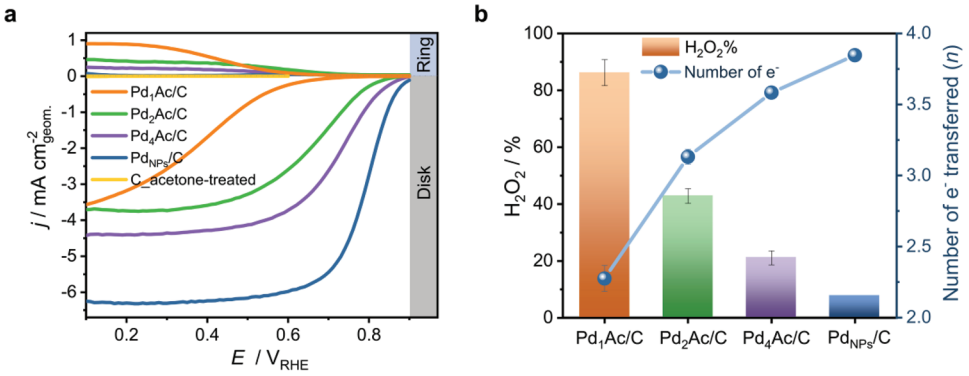

Figure 2. ORR performance of Pd_xAc/C catalysts. a) RRDE voltammograms obtained in an O_2-saturated 0.1 M $HClO_4$ electrolyte with a scan rate of 10 mV s^{-1} at 1600 rpm (only the cathodic scan is shown), together with the detected H_2O_2 current density on the ring electrode (upper panel) at a fixed potential of 1.4 V_{RHE}. The Pd loading on the electrode was fixed at 10 μg cm^{-2}. b) H_2O_2 selectivity and the number of electrons derived from RRDE data.

On these surfaces, hydrogen peroxide can be further reduced to water, thereby reducing the selectivity for H_2O_2 in a competitive manner.[15–17]

As the proportion of metal clusters and nanoparticles increased, the reaction increasingly favors a 4-electron transfer. To discriminate between genuine homogeneous molecular catalysis and cluster/nanoparticle catalysis, it is desirable to selectively block one of the catalytic sites. In this regard, we employed CO as a probe molecule. The utilization of CO as a probe draws inspiration from previously reported methodologies such as the mercury poisoning test[14] and halide adsorption, [37,38] given its robust adsorption characteristics on noble metals with extended surfaces, including platinum (Pt) and Pd.[39]

The adsorption energies of CO are known to exhibit variability depending on the specific interaction sites, with lower energies typically observed for on-top binding sites, and higher energies associated with bridge and hollow sites.[40–42] Qiao et al. investigated the nature of single atom Pt supported on FeO_x by employing in situ IR spectra of CO adsorption complemented by DFT calculation. The authors observed that CO adsorption on single $Pt^{\delta+}$ atoms is weak and partially reversible. In contrast, on Pt-dimers or Pt clusters, CO adsorption in a bridge-bonded configuration was found to be irreversible, persisting even after evacuation in vacuo.[43] This distinct difference in CO adsorption behavior allowed for the selective blocking of active sites on larger Pd clusters (Pd_x, $x > 2$). Consequently, this approach enables the estimation of catalytic performance specifically attributed to isolated Pd single atoms.

To mitigate electrochemical oxidation of adsorbed CO, the ORR measurements were conducted within a narrow potential window of 0.1 to 0.5 V_{RHE}, as illustrated in **Figure 3**a and Figure 3b. Upon CO adsorption on the catalyst surface, the mass-normalized current taken at 0.4 V_{RHE} for Pd_1Ac/C exhibited a partial decrease from 0.20 to 0.11 mA μg^{-1}. Simultaneously, the selectivity was significantly enhanced to 95%. Similar trends were observed for Pd_2Ac/C, Pd_4Ac/C, and the reference Pd_{NPs}/C, where the ORR activity decreased while the H_2O_2 selectivity increased, reaching values of 95%, 96%, and 92%, respectively. A decrease in mass normalized current was observed for Pd_2Ac/C and Pd_4Ac/C, ranging from 0.36 to 0.08 and from 0.43 to 0.05 mA μg^{-1}. In contrast, the reference catalyst Pd_{NPs}/C exhibited a substantial decrease in activity from 0.10 to 0.02 mA μg^{-1}, which is likely due to the coverage of CO on the extended surface of Pd. For Pd_xAc/C, the modified catalytic performance and manipulated reaction path from $4e^-$ to $2e^-$ ORR can be attributed either to the exposure of only active sites of Pd single atom, achieved by fully blocking the active site of clusters in the mixed single atom and cluster system, or to the interaction not only with the active sites of Pd single atoms but also with the partially unblocked active site of clusters. While it is challenging to determine whether the adsorbed CO fully or partially covers the active sites of clusters, we believe that the presence of acetylacetonate ligands hinders oxygen access to the unblocked active sites of the clusters that might remain after CO adsorption. In the case of partially reduced metallic Pd in the bigger sized clusters after ORR, as demonstrated in Figures S3 and S4 (Supporting Information), the unblocked sites, on which CO is relatively weakly adsorbed, can also contribute to changing the reaction pathway due to the absence of steric effects caused by acetylacetonate ligands. However, as depicted in Figure 3a, metallic Pd nanoparticles significantly lost their activity after CO adsorption. Based on this observation, the contribution of reduced metallic Pd derived from the bigger sized clusters after ORR to the manipulated reaction pathway is minuscule compared to that from the single Pd atoms. As a result, we can cautiously conclude that the altered reaction pathway observed after CO adsorption primarily originates from the single atom Pd surfaces, where their active sites remain in the mixed single atom and cluster system of Pd_xAc/C. This observed selectivity of CO to selectively block active sites on extended surfaces, thereby leaving only single sites as catalytic centers, provides valuable insights in how to deliberately modulate the ORR performance. Consequently, there is a reduction in electron transfer to 2.1 for all Pd_xAc/C catalysts which is consistent with the proposed mechanistic model.

In Figure S5 (Supporting Information), the CO stripping behavior is shown for our different catalyst systems. We note a minimal CO stripping peak, indicating that there is limited hindrance in CO adsorption and that CO ad/desorption on the active sites of single atoms is reversible and weak, thereby supporting our initial hypothesis. As the size of the clusters increases, the CO stripping peaks become more pronounced indicating a higher share of extended surfaces. However, relying solely on the

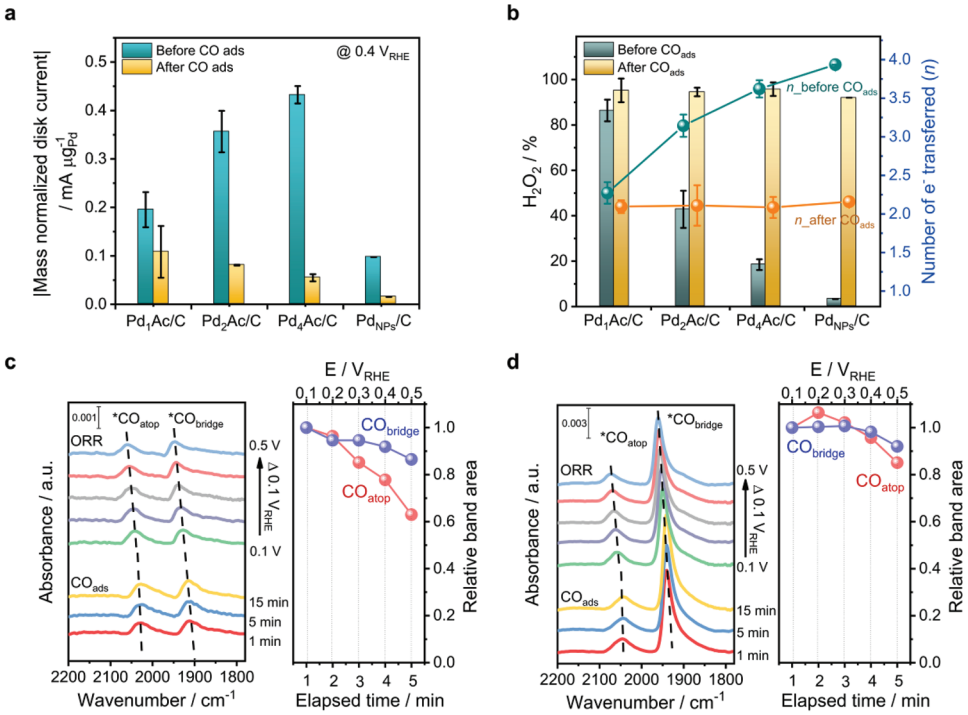

Figure 3. Effect of CO adsorption on Pd_xAc/C catalysts. a) Comparison of ORR activities (before and after CO adsorption) at 0.4 V_{RHE} measured by RRDE in an O_2-saturated 0.1 M $HClO_4$ electrolyte from 0.1–0.5 V_{RHE} at 1600 rpm. b) H_2O_2 production selectivity and the number of electrons estimated by RRDE measurements. c,d) Series of time-dependent in-situ/operando EC ATR-SEIRAS spectra collected during CO adsorption at −0.2 V_{RHE} and ORR at applied potential in 0.1 M $HClO_4$ for Pd_1Ac/C (left panel (c)) and Pd_4Ac/C (left panel (d)) and response of the integrated band areas for CO_{atop} and CO_{bridge} during the ORR (right panel (c,d)).

interpretation of the CO stripping behavior has its limitations. These curves provide information about the total amount of adsorbed CO on extended surfaces but do not offer precise insights into the extent of blockage for different-sized Pd_xAc/C catalysts.

To overcome this limitation and gain deeper understanding regarding the influence of CO adsorption on catalytic performance, we employed in-situ/operando EC ATR-SEIRAS for both Pd_1Ac/C and Pd_4Ac/C catalysts. This technique allows us to obtain more comprehensive insights into the impact of CO adsorption on the catalysts' behavior. Both catalysts were selected as they exhibit the highest proportion of single atoms (Pd_1Ac/C) or clusters (Pd_4Ac/C), respectively. The obtained spectra, as shown in Figure 3c, d, and Figure S4 (Supporting Information), reveal distinctive CO absorption features. The observed high-frequency peaks in the range of 2150–2000 cm^{-1} indicate linearly bonded CO on atop Pd atoms. In contrast, the low-frequency peaks observed in the range of 2000–1800 cm^{-1} correspond to CO species bound in bridge position (2000–1895 cm^{-1}) or in threefold coordination (1920–1830 cm^{-1}) on extended Pd surfaces or clusters.[44]

The left panel of Figure 3c, two prominent CO bands are observed at frequencies of 2040 cm^{-1} and 1939 cm^{-1}. These bands are assigned to linearly bonded CO (CO_{atop}) on atop sites of Pd single atoms and bridge-bonded CO (CO_{bridge}) on Pd clusters in Pd_1Ac/C. This observation was made during the introduction of CO into the electrolyte and the subsequent CO adsorption process at a potential of −0.2 V_{RHE}. No threefold bound CO species were detected. For Pd_4Ac/C, as depicted in Figure 3d, both CO_{atop} and CO_{bridge} are present, appearing at frequencies of 2041 and 1939 cm^{-1}, respectively. While the intensity of CO_{atop} and CO_{bridge} is relatively similar for Pd_1Ac/C, the CO_{bridge} peak is notably more intense than the CO_{atop} peak for Pd_4Ac/C. This observation suggests a higher proportion of clusters or nanoparticles in the catalyst, consistent with our electron microscopy findings. The observed 1 cm^{-1} blue shift in the CO_{atop} band of Pd_4Ac/C compared to Pd_1Ac/C indicates a small variation in dipole–dipole coupling or the electronic structure of Pd.[45] As expected, the peak positions of CO_{atop} and CO_{bridge} exhibit a blue shift with increasing positive applied potential for both Pd_1Ac/C and Pd_4Ac/C, a phenomenon known as the vibrational Stark effect.[46]

In the right panels of Figure 3c,d, the effect of introducing O_2 at the applied potential, on the CO bands is observed. For Pd_1Ac/C, the relative area of the CO_{atop} band decreases significantly by 37% upon O_2 introduction. On the other hand, Pd_4Ac/C exhibited only a slight decrease in relative area indicating a time dependency of CO desorption at loosely bound single atom centers in the presence of O_2. In contrast to the behavior of CO_{atop}, the relative CO_{bridge} band intensity remains largely unchanged during the ORR for both catalysts, indicating that CO_{bridge} is a more irreversibly adsorbed species that blocks the active sites of the cluster surface and hinders the initiation of the ORR.

The quantification of the CO_{atop} to CO_{bridge} peak ratio allows for the estimation of the relative populations of Pd single atoms and cluster/nanoparticles on the surfaces of Pd_xAc/C catalysts. As depicted in **Figure 4**a, following a 15-min CO adsorption period, integrated area ratio of CO_{atop} to CO_{bridge} is found to be 0.76

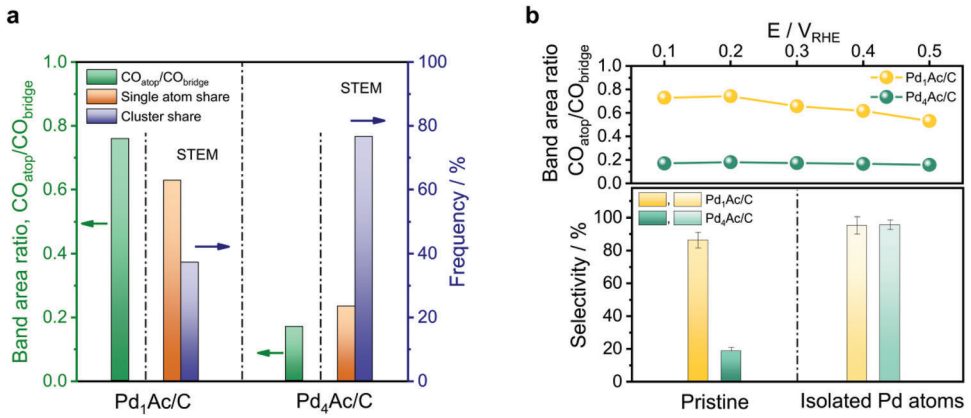

Figure 4. a) Correlation between the band area ratio of CO_{atop} to CO_{bridge} with the frequency of Pd single atoms and clusters in the catalysts and b) H_2O_2 selectivity before (pristine) and after deactivation (isolated Pd atoms) of the clusters by CO.

for Pd_1Ac/C and 0.17 for Pd_4Ac/C. These ratios align well with the particle size distribution analyzed by STEM. This correlation indicates that a higher proportion of CO_{atop} is present when the catalysts consist of a larger proportion of single atoms, as observed in Pd_1Ac/C, which exhibits higher mass activity following CO adsorption.

By correlating the relative abundance of CO_{atop} and CO_{bridge} to the product selectivity (Figure 4b), a greater population of CO_{atop} promotes the preferential reduction of O_2 to H_2O_2. The presence of predominantly adsorbed CO on bridge sites shifts the ORR toward the production of H_2O at Pd single atoms and Pd clusters. The introduction of CO as a blocking agent on the catalyst surface enables the selective deactivation of specific sites on Pd improving the H_2O_2 selectivity up to 95% and 96% for Pd_1Ac/C and Pd_4Ac/C, respectively. By manipulating the adsorption behavior of CO, it becomes possible to isolate Pd single atoms and effectively modulate the ORR pathway, favoring the production of H_2O_2.

3. Conclusion

We have shown how sub-nanometer sized Pd particles can be engineered to have high selectivity toward H_2O_2. To discriminate between genuine homogeneous molecular catalysis and cluster/nanoparticle catalysis, a new methodology based on CO as probe molecule was introduced. This approach effectively prevented the over-reduction to H_2O allowing for the quantification of single atom active sites, while at the same time modulate the performance of the active species. In-situ/operando electrochemical infrared spectroscopy revealed the substantially different adsorption behavior of CO on single and cluster sites as well as on extended surfaces on nanoparticles. Notably, a single atom-based catalyst demonstrated selectivities up to 96% in rotating ring disk electrode measurements over the potential range between 0.1 and 0.5 V_{RHE}. This unique performance arises specifically from the high amount of CO_{atop} adsorption and the lack of CO_{bridge} sites. By leveraging the ability to control the size, composition, and environment of metal clusters and single atoms, we can devise promising design strategies for sustainable and efficient catalytic processes.

Supporting Information

Supporting Information is available from the Wiley Online Library or from the author.

Acknowledgements

J.S.C., E.S.K., and M.L. acknowledge the Federal Ministry of Education and Research (BMBF) in the framework of NanoMatFutur (SynKat, FK: 03XP0265) for financial support. S.Y. and Y.J.H. acknowledge the support by the Institute for Basic Science (IBS-R006-D1) and Creative-Pioneering Researchers Program through Seoul National University. G.V.F. and M.R.V.L. would like to express their gratitude to the São Paulo Research Foundation (FAPESP – grants #2017/10118-0, #2019/04421-7, and # 2021/14194-8) and Brazilian National Council for Scientific and Technological Development (CNPq – grants#465571/2014-0 and #303943/2021-1).

Open access funding enabled and organized by Projekt DEAL.

Conflict of Interest

The authors declare no conflict of interest

Data Availability Statement

The data that support the findings of this study are available from the corresponding author upon reasonable request.

Keywords

hydrogen peroxide, in situ ATR-SEIRAS, oxygen reduction reaction, size effects, sub-nano scale

Received: August 17, 2023
Revised: September 11, 2023
Published online: September 29, 2023

[1] W. Xiaoqian, L. Zhijun, Q. Yunteng, Y. Tongwei, W. Wenyu, W. Yuen, L. Yadong, *Chem* **2019**, *5*, 1486.

[2] M. Nesselberger, M. Roefzaad, R. Fayçal Hamou, P. Ulrich Biedermann, F. F. Schweinberger, S. Kunz, K. Schloegl, G. K. H. Wiberg, S. Ashton, U. Heiz, K. J. J. Mayrhofer, M. Arenz, *Nat. Mater.* **2013**, *12*, 919.
[3] S. Taylor, E. Fabbri, P. Levecque, T. J. Schmidt, O. Conrad, *Electrocatalysis* **2016**, *7*, 287.
[4] A. Verdaguer-Casadevall, D. Deiana, M. Karamad, S. Siahrostami, P. Malacrida, T. W. Hansen, J. Rossmeisl, I.b Chorkendorff, I. E. L. Stephens, *Nano Lett.* **2014**, *14*, 1603.
[5] L. Lu, S. Zou, Y. Zhou, J. Liu, R. Li, Z. Xu, L. Xiao, J. Fan, *Catal. Sci. Technol.* **2018**, *8*, 746.
[6] C. H. Choi, M. Kim, H. C. Kwon, S. J. Cho, S. Yun, H.-T. Kim, K. J. J. Mayrhofer, H. Kim, M. Choi, *Nat. Commun.* **2016**, *7*, 10922.
[7] M. Shao, A. Peles, K. Shoemaker, *Nano Lett.* **2011**, *11*, 3714.
[8] H. Yin, H. Tang, D. Wang, Y. Gao, Z. Tang, *ACS Nano* **2012**, *6*, 8288.
[9] S. Yang, J. Kim, Y. J. Tak, A. Soon, H. Lee, *Angew. Chem., Int. Ed.* **2016**, *55*, 2058.
[10] X. Guo, S. Lin, J. Gu, S. Zhang, Z. Chen, S. Huang, *ACS Catal.* **2019**, *9*, 11042.
[11] Q. Chang, P. Zhang, A. H. B. Mostaghimi, X. Zhao, S. R. Denny, J. H. Lee, H. Gao, Y. Zhang, H. L. Xin, S. Siahrostami, J. G. Chen, Z. Chen, *Nat. Commun.* **2020**, *11*, 1.
[12] G. V. Fortunato, M. S. Kronka, A. J. Dos Santos, M. Ledendecker, M. R. V. Lanza, *Chemosphere* **2020**, *259*, 127523.
[13] V. M. Chernyshev, A. V. Astakhov, I. E. Chikunov, R. V. Tyurin, D. B. Eremin, G. S. Ranny, V. N. Khrustalev, V. P. Ananikov, *ACS Catal.* **2019**, *9*, 2984.
[14] G. M. Whitesides, M. Hackett, R. L. Brainard, J. P. P. M. Lavalleye, A. F. Sowinski, A. N. Izumi, S. S. Moore, D. W. Brown, E. M. Staudt, *Organometallics* **1985**, *4*, 1819.
[15] M. Inaba, A. Zana, J. Quinson, F. Bizzotto, C. Dosche, A. Dworzak, M. Oezaslan, S. B. Simonsen, L. T. Kuhn, M. Arenz, *ACS Catal.* **2021**, *11*, 7144.
[16] G. V. Fortunato, E. Pizzutilo, A. M. Mingers, O. Kasian, S. Cherevko, E. S. F. Cardoso, K. J. J. Mayrhofer, G. Maia, M. Ledendecker, *J. Phys. Chem. C* **2018**, *122*, 15878.
[17] L. Zhang, T. Yang, W. Zang, Z. Kou, Y. Ma, M. Waqar, X. Liu, L. Zheng, S. J. Pennycook, Z. Liu, X. J. Loh, L. Shen, J. Wang, *Adv. Sci.* **2021**, *8*, 1.
[18] M. Shao, Q. Chang, J.-P. Dodelet, R. Chenitz, *Chem. Rev.* **2016**, *116*, 3594.
[19] G. A. Tritsaris, J. Greeley, J. Rossmeisl, J. K. Nørskov, *Catal. Lett.* **2011**, *141*, 909.
[20] M. Nesselberger, S. Ashton, J. C. Meier, I. Katsounaros, K. J. J. Mayrhofer, M. Arenz, *J. Am. Chem. Soc.* **2011**, *133*, 17428.
[21] K. J. J. Mayrhofer, B. B. Blizanac, M. Arenz, V. R. Stamenkovic, P. N. Ross, N. M. Markovic, *J. Phys. Chem. B* **2005**, *109*, 14433.
[22] T. Mittermeier, A. Weiß, H. A. Gasteiger, F. Hasché, *J. Electrochem. Soc.* **2017**, *164*, F1081.
[23] M. Inaba, H. Yamada, J. Tokunaga, A. Tasaka, *Electrochem. Solid-State Lett.* **2004**, *7*, 474.
[24] E. Fabbri, S. Taylor, A. Rabis, P. Levecque, O. Conrad, R. Kötz, T. J. Schmidt, *ChemCatChem* **2014**, *6*, 1122.
[25] T. W. Huang, M. Nagayama, J. Matsuda, K. Sasaki, A. Hayashi, *Molecules* **2021**, *26*, 724.
[26] X. Sun, S. R. Dawson, T. E. Parmentier, G. Malta, T. E. Davies, Q. He, L. Lu, D. J. Morgan, N. Carthey, P. Johnston, S. A. Kondrat, S. J. Freakley, C. J. Kiely, G. J. Hutchings, *Nat. Chem.* **2020**, *12*, 560.
[27] K. Noack, H. Zbinden, R. Schl?Gl, *Catal. Lett.* **1990**, *4*, 145.
[28] A. R. Mouat, C. L. Whitford, B.-R. Chen, S. Liu, F. A. Perras, M. Pruski, M. J. Bedzyk, M. Delferro, P. C. Stair, T. J. Marks, *Chem. Mater.* **2018**, *30*, 1032.
[29] W. Xiao, M. A. Liutheviciene Cordeiro, M. Gong, L. Han, J. Wang, C. Bian, J. Zhu, H. L. Xin, D. Wang, *J. Mater. Chem. A* **2017**, *5*, 9867.
[30] D. Alba-Molina, A. R. Puente Santiago, J. J. Giner-Casares, E. Rodríguez-Castellón, M. T. Martín-Romero, L. Camacho, R. Luque, M. Cano, *J. Mater. Chem. A* **2019**, *7*, 20425.
[31] G. M. Lari, B. Puértolas, M. Shahrokhi, N. López, J. Pérez-Ramírez, *Angew. Chem., Int. Ed.* **2017**, *56*, 1775.
[32] L. F. De Freitas, B. Puértolas, J. Zhang, B. Wang, A. S. Hoffman, S. R. Bare, J. Pérez-Ramírez, J. W. Medlin, E. Nikolla, *ACS Catal.* **2020**, *10*, 5202.
[33] A. Kulkarni, S. Siahrostami, A. Patel, J. K. Nørskov, *Chem. Rev.* **2018**, *118*, 2302.
[34] M. Song, M. Chen, C. Zhang, J. Zhang, W. Liu, X. Huang, J. Li, G. Feng, D. Wang, *ACS Appl. Mater. Interfaces* **2023**, *15*, 31375.
[35] M. M. Montemore, M. A. Van Spronsen, R. J. Madix, C. M. Friend, *Chem. Rev.* **2018**, *118*, 2816.
[36] Z. Ma, Z. P. Cano, A. Yu, Z. Chen, G. Jiang, X. Fu, L. Yang, T. Wu, Z. Bai, J. Lu, *Angew. Chemie Int. Ed.* **2020**, *59*, 18334.
[37] G. V. Fortunato, E. Pizzutilo, E. S. F. Cardoso, M. R. V. Lanza, I. Katsounaros, S. J. Freakley, K. J. J. Mayrhofer, G. Maia, M. Ledendecker, *J. Catal.* **2020**, *389*, 400.
[38] P. Priyadarshini, T. Ricciardulli, J. S. Adams, Y. S. Yun, D. W. Flaherty, *J. Catal.* **2021**, *399*, 24.
[39] I. J. Mcpherson, P. A. Ash, L. Jones, A. Varambhia, R. M. J. Jacobs, K. A. Vincent, *J. Phys. Chem. C* **2017**, *121*, 17176.
[40] V. Bertin, E. Agacino, R. López-Rendon, E. Poulain, *J. J. Mol. Struct.: THEOCHEM* **2006**, *769*, 243.
[41] B. D. Adams, R. M. Asmussen, A. Chen, R. C. Mawhinney, *Can. J. Chem.* **2011**, *89*, 1445.
[42] P. Ferrari, G. Libeert, N. M. Tam, E. Janssens, *CrystEngComm* **2020**, *22*, 4807.
[43] B. Qiao, A. Wang, X. Yang, L. F. Allard, Z. Jiang, Y. Cui, J. Liu, J. Li, T. Zhang, *Nat. Chem.* **2011**, *3*, 634.
[44] N. E. Kolli, L. Delannoy, C. Louis, *J. Catal.* **2013**, *297*, 79.
[45] T. Ricciardulli, S. Gorthy, J. S. Adams, C. Thompson, A. M. Karim, M. Neurock, D. W. Flaherty, *J. Am. Chem. Soc.* **2021**, *143*, 5445.
[46] D. Bhattacharyya, P. E. Videla, M. Cattaneo, V. S. Batista, T. Lian, C. P. Kubiak, *Chem. Sci.* **2021**, *12*, 10131.